Development of standardized fracture model for tibial plateau fractures with full soft tissue mantle

Justin Combs

***Abstract*—Standardized fracture models are utilized to create life-like fractures in synthetic or cadaveric bones, which are then used for surgical training courses. The present paper presents a standardized fracture model for producing a variety of tibial plateau fracture patterns with minimal soft tissue damage. A custom-built drop tower was constructed to support the leg specimen and allow for axial compression of PMMA embedded femoral shafts. Through the implementation of a high-energy axial-impulse compression, abduction and adduction of the knee, and cortical bone weakening to predetermine the fracture breaking point, the desired fracture patterns were produced in cadaveric specimen. The results show that it is possible to produce a variety of fracture types, each presenting with a distinct fracture pattern that mimic those of natural injury mechanisms. The resulting fractures also presented with expected concomitant injuries seen in in vivo tibial plateau fractures. Three fracture patterns were produced, including a lateral split-depression fracture, a medial split with lateral depression, and a bicondylar split fracture. In the 24 tested specimen, $12.50\,\%$ (n=3) resulted in a lateral split pattern, $45.83\,\%$ (n=11) in a bicondylar fracture pattern, and $37.50\,\%$ (n=9) in a medial fracture pattern. One specimen $4.17\,\%$ resulted in an undesired fracture pattern. The average energy threshold needed to produce a fracture was $51.25\,\mathrm{J}\pm12.08$ and the specimens had a mean BMD of $106.22\,\mathrm{mg/cm^3}\pm45.51$. This fracture model allows for more realistic training on life-like fractures, with the surgical field integrity being maintained and associated concomitant injuries being produced.**

***Index Terms*—Fracture model, Tibial plateau, surgical education, knee.**

I. Introduction

THE knee joint is fundamental to quality of life and locomotion. It ensures stability and assists with balance and gait. Injuries to the knee, whether age-related or from trauma, typically result in severely compromised daily activities. This joint is composed of the distal end of the femur, the proximal end of the tibia, the patella, and various ligaments encapsulated by synovial fluid. The bones, ligaments, and muscles interact in complex ways, allowing for the management of the biomechanical demands of the knee. Fractures to the bones involved can typically be classified as intra- or extra-articular. The tibial plateau is considered intra-articular. Tibial plateau fractures (TPFs) account for $56.9\,\%$ [1] of all fractures in elderly persons and around $1\,\%$ of all long-bone fractures [2]. The distal end of the femur is made up of the lateral and medial condyles, both of which have a convex, ellipsoidal shape of increasing curvature as the curve moves posteriorly. The two femoral condyles are separated by the intercondylar notch, a slight notch in the middle of the distal femur. The femoral shaft extends upwards from the condyles, with a varus tilt that is between 5-7° stated in literature [3], [4]. Varus tilt means angling laterally in regards to the sagittal plane; conversely a valgus tilt is tilting medially. The lowest point of the medial femoral condyle is distal to the lowest point of the lateral condyle [2], [5]. The femoral condyles articulate directly with the tibial condyles.

The proximal tibial is composed of the lateral and medial condyles, the tibial tuberosity, Gerdy's tubercle, and the eminentia intercondylaris, a bony protrusion that juts out from the center of the tibial plateau and fits into the fossa intercondylaris with normal knee alignment [2]. The lateral plateau sits slightly proximal to the medial plateau and has a slightly convex curvature. Opposingly, the medial plateau has a slightly concave curvature. The concavity of the medial plateau allows for a better congruity with the medial femoral condyle and bears approximately $60\,\%$ [2] of the weight borne to the tibial plateau.

The injury mechanisms for TPFs are greatly age dependent, with the majority of injuries in elderly people resulting from falls from standing height [6]; yet the most common injury mechanisms for younger people is high-energy trauma [2], such as from a mountain biking or skiing accident, or vehicular collisions. Lower bone mineral density and osteoporotic diseases contribute highly to the fractures resulting from low-energy trauma in elderly populations, and is evident from the resulting fracture patterns [1], [2]. However, regardless of the particular injury mechanism, proper reduction is necessary in TPFs to restore proper function of the knee. Kim et al. defines reduction loss, or failure of the surgical fixation, as a "depression of the articular surface that is greater than 3mm compared to the immediate postoperative radiographs, a condylar widening that is greater than 5mm, and an alignment change that is greater than 5° towards the varus or valgus" [7]. Additionally, breakage or loosening of the fixation plate is considered a reduction loss. Kim et al. also claims that fracture pattern is a key factor in reduction loss when deciding the fixation method or surgical approach, and Weaver et al. found that certain fracture patterns have reduction loss in bicondylar fractures to have reported incidences of 29-59 % [8].

With this in mind, proper classification of the fracture pattern is of high importance. One of the first methods for classifying TPFs is the Hohl-Moore classification system, which has been widely adopted. Other prevalent classification systems include the Schatzker system and the system from AO Foundation/Orthopedic Trauma Association (AO/OTA). No one system has become the gold standard and a number of studies have shown that there is poor reproducibility in many of the

J. Combs is with the Department of Medical and Health Technologies, MCI, Innsbruck, Austria, e-mail: justin.combs@mci.edu.

Manuscript received July 27, 2023; revised July 29, 2023.

classification systems, with both inter- and intrapersonal discrepancies when classifying the same fracture from radiologic images 8 weeks after fist classifying it [9]–[11]. When looking at published literature, a new classification system for tibial plateaus has been proposed every few years since the early 2000's, yet the AO/OTA classification system is still the most widely accepted globally [10], [11].

Regardless of the classification system chosen, the top influence of reduction loss is the surgical fixation of the TPF. As such, surgeons need to train and perform numerous reductions of a variety of fracture patterns to be properly prepared to give each patient the best care possible. Thus there is a need for surgical training and surgical training courses, both during training and post board certifications. Though synthetic bones are great for training screw placement or plate fixation, they fail to include the concomitant soft tissue injuries common with TPFs. Cadaveric specimens can fill this void. Wegmann et al. discusses the need for life-like fractures in cadaveric specimens [12], [13]. To date, there are no reliable methods of producing TPFs with an intact soft tissue envelope. From discussions with surgeons and a review of the literature, the current methods of producing TPFs are to cut open the knee joint, expose the tibial plateau, and use a rotary saw or a chisel to produce the desired fracture patterns [1], [3], [8], [14].

The objective of this paper is to propose a reliable and reproducible method of producing tibial plateau fractures in cadaveric specimen with minimal damage to the soft tissue envelope. A combination of loading with a high energy impact and cortical weakening to predetermine fracture points are to be used. Producing a variety of fracture patterns is desired, as the cadaver specimens will be returned to the Medical University of Innsbruck for use in surgical training courses on reduction of tibial plateau fractures.

II. Methods

A. Specimen Preparation

Two different types of cadaveric specimen were used for this research project, both obtained from the Anatomy Department of the Medical University of Innsbruck. All donors signed a waiver during their life, choosing to donate their body to the University for scientific research. In the pilot study for this project, nine fresh-frozen isolated knee specimens were available in the biomechanics laboratory. These nine had been used in a previous project testing ACL repair techniques and graft insertion techniques. As such, each specimen had tunnels drilled into the tibial and femoral condyles, the skin and subcutaneous tissue had been removed, and a number of ligaments and tendons had been severed and sutured together. Additionally, the specimens had been embedded at the tibial shaft and the femoral shaft. This precludes the nine specimens from the current investigation, yet their use in the pilot study provided vital insight into the necessary energy for fracture creation and cortical bone weakening for determination of fracture patterns and fracture line breaking points in the tibial plateau. Due to their preclusion, data on these specimen is not presented in the present paper.

For the main test series of the present research, 24 ethanol-glycerine fixed specimens were obtained. These specimens were near complete lower extremities, cut at the middle of the femoral shaft. The foot and ankle joints were intact and pre-screening by radiographic imaging was performed to preclude any specimens with prior knee surgeries. These specimen were embedded in polymethylmethacrylate (PMMA) (Technovit 3040; Kulzer GmbH, Wehrheim, Germany). After embedding, the specimen were prepared for fracture creation. Utilizing a C-arm X-ray machine (ARCADIS Varic, SIEMENS, Munich, Germany), the coronal portion of the tibial plateau was identified. Two small incisions of roughly $1.5\,\mathrm{cm}$ were made on the anterior and posterior side of the knee joint. Using a chisel and hammer, the cortical bone of the tibial plateau was weakened in a defined pattern for the desired fracture pattern. Care was taken to avoid excessive chiseling and damage to the trabecular bone of the epiphysis and metaphysis of the proximal tibia. After chiseling, X-rays were saved showing the chisel location and cortical weakening pattern for each specimen. The specimens were then ready for fracture creation.

B. Experimental Design

The test bench used for this project was constructed out of aluminum profiles (Profile 8 $40\mathrm{x}40\mathrm{mm}$, Item, Solingen, Germany) and measure $42\mathrm{x}42\mathrm{x}200\mathrm{cm}$. A guide rail is positioned at what is determined to be the back of the bench, allowing for a smooth, low-friction fall of the sledge. The sledge extends from the guide rail and has a stainless-steel impactor on the bottom portion, and a rod for weights to be affixed and secured on the top of it. A uniaxial accelerometer (B&K 4516, Brüel and Kjaer, Nærum, Denmark) rated to $\pm 1000\,\mathrm{g}$ was affixed to the impactor per the manufacturers instructions. The sampling frequency was set to $51.200\,\mathrm{Hz}$. A compact Data Aquisition box (cDAQ NI 9234, National Instruments Corporation, Austin, TX, USA) was used to collect the sensor reading. More information is available in the Data Collection subsection.

Specimen positioning begins with placing the chiseled specimen into a plastic bag and securing this above the top of the remaining soft tissue around the exposed femur. The specimen is then placed in the tower, inserting the PMMA embedding into the guidance ring from underneath. The height of the guidance ring is adjusted to fit the specimen, then the foot is secured to the baseplate. Two sliding L-shaped pieces fix the foot from moving laterally or posteriorly, and they angle and squeeze from the ball of the foot to the heel. An aluminium bar is secured over the top of the foot, with a rubber cushion between the metal and specimen, to prevent the foot from sliding forward. Ratchet straps and tension straps are then wrapped around the specimen, beginning at the femur to get it into the desired position. The femur should be straight to allow for easy movement of the PMMA through the guidance ring. Afterwards straps are lashed around the tibia, above the belly of the gastrocnemius (calf muscle) and around the ankle. The desired valgus or varus angulation is made by tensioning

the upper and lower tibia straps, taking care to avoid rotation of the specimen while inducing the tibiofemoral angulation. Afterwards, the mechanical stop is positioned so that the sledge does not impact the guidance ring and force excessive displacement of the femur.

A guidance ring was added to the test bench to restrict the movement of the femoral embedding, ensuring direct translation of the induced energy. A second guide rail was added across from the first to stabilize the sledge. As this testing is based on axial compression, a load is added to the sledge, raised to a predetermined height, then dropped to allow for a jarring, high energy impact on the femur, mimicking the natural injury mechanisms. By changing the weight applied and the height to which the sledge is raised, there is a linear progression of the theoretical energy induced into the system.

$$P.E. = (mass)(height)(g) \tag{1}$$

$$ResultingEnergy = (mass_{added})(height)(accel) \tag{2}$$

To determine the total mass, the sledge was removed from the system and weighed ($3.98\,\mathrm{kg}$). A drop height of $40\,\mathrm{cm}$ and a total mass of $15.5\,\mathrm{kg}$ was used as the starting point for most specimens, with the drop height being measured from the top of the femoral embedding to the bottom of the impactor. This location was marked on the guide rail during the positioning of the specimen. The actual acceleration due to gravity was measured by the accelerometer, with the mean being $5.95\,\mathrm{m/s^2} \pm 0.67$.

C. Fracture Patterns

A conversation with a senior surgeon from the Orthopaedic and Traumatology Department of the Medical University of Innsbruck lead to the definition of three desirable fracture patterns. An approximation of each fracture pattern was drawn on synthetic tibiae. The nine fresh-frozen specimen used in the pilot study assisted in the refinement of the cortical weakening for each fracture pattern. By chiseling through the crown and articular surface of the tibial plateau, breaking points for the condylar fractures were predetermined. It is worth iterating that the chiseling is intended only to weaken the cortical bone of the proximal tibia. Chiseling deep into the trabecular bone should be avoided, yet the chisel marks at the crown of the tibial plateau must completely bisect the the articular surface's cortical bone of the proximal tibia.

1) Fracture Pattern 1: Lateral Split with Lateral Depression: This fracture pattern can be classified by the AO classification as a "41-B3.1." It is desired that the entire lateral condyle is contained in the split. To achieve this, cortical weakening is performed such that a line is chiseled through the tibial plateau just medial to the lateral condyle and just lateral to the intercondylar eminence. A $1.5\,\mathrm{cm}$ is made lateral to the patellar tendon, beginning at the inferior point of the patella and traversing inferior for the distance of the incision. The lateral condyle anterior rim is then identified and the chisel positioned under radiographic guidance by the C-arm prior to chiseling. The chisel should be partially in the joint space and partially within the tibial plateau, hammered such that it moves parallel to the lateral articular surface and reaches a depth of approximately the midpoint of the intercondylar eminence. A posterior incision of the same size is made in the popliteal fossa to allow for identification of the popliteal notch and the posterior edge of the lateral condyle. Again under X-ray guidance, the chisel is hammered parallel to the lateral articular surface to reach the midpoint of the intercondylar eminence.

2) Fracture Pattern 2: Bicondylar Split: This fracture pattern can be classified by the AO classification as a "41-C3" with two fractures of the articular surface. To prepare for this fracture the cortical bone is weakened in an X shape. Initially, after making a $1.5\,\mathrm{cm}$ incision lateral of the patellar tendon, two chisel lines are made on either side of the intercondylar eminence. Afterwards, the chisel is placed at the anterior aspect of the lateral chisel groove and angled in such a way that it is pointed distally and medially. A line is chiseled through the anterior intercondylar space and to the medial side of the tibial tuberosity. A second line is chiseled through the cortical bone traversing from the medial chisel line to the lateral side of the tibial tubercle. The resulting chisel lines should for an "X" with its intersection point placed between the superior edge of the tibial tubercle and the anterior intercondylar space. A posterior incision is made in the popliteal fossa and a similar "X" shape is chiseled into the posterior tibia, extending from either articular chisel line, through the popliteal notch, and into the posterior intercondylar space and towards the opposite side of the tibia.

3) Fracture Pattern 3: Medial Split with Lateral Depression: This fracture pattern can be classified as a "41-B3.3" and it is desired that the intercondylar eminence is part of the split fragment. A $1.5\,\mathrm{cm}$ incision is made at the anteromedial aspect of the knee, beginning at the inferior edge of the patella. After identifying the medial condylar rim, the chisel is positioned from the anterior aspect of the medial condyle and aimed towards the anterolateral corner of the intercondylar eminence under X-ray guidance. A line is chiseled through the anterior intercondylar space, passing posteriorly to the tibial tubercle, to reach the lateral aspect of the intercondylar eminence. Posteriorly, an incision is made in the popliteal fossa and the chisel hammered lateral to the intercondylar eminence, yet medial to the lateral condyle's articular surface, to reach the anterior aspect of the intercondylar eminence, intersecting the anterior chisel line.

D. Data Collection and Analysis

Once positioned, the piezoelectric acclerometer was initialized and checked by running the written MATLAB (MATLAB Software 2023a, The MathWorks, Natick, USA, 2023) live script. When running, the script samples at a $51.2\,\mathrm{kHz}$ frequency for $5\,\mathrm{s}$ duration. During this time, the sledge was manipulated by hand to produce some movement. After running, a plot of the acceleration was displayed. If the resulting graph matched the movement induced, then testing began. If not, the sensor was re-initialized, once again checking to see if the expected movement was recorded and

displayed accordingly.
When ready to test, the sledge was raised to the determined height, then the recording started. The experimenter held the sledge suspended for roughly $2\,\mathrm{s}$ prior to dropping the sledge. After impact, the specimen and tower were left untouched until the sampling time ended. The acceleration was then plotted and the data and graphs saved.
After the drop test was complete, the specimen were imaged again with the C-arm to check if a fracture was produced. Specimen were imaged anteriorly and from either a lateral or medial perspective, dependent upon the desired fracture. Images of the resulting fractures were saved with a file name corresponding to the saved drop test data. The hard copy of the test protocol was filled in, detailing and recording any and all deviations, as well as notes and ideations on the resulting fractures. If no fracture was seen, the specimen was subjected to further impacts of increasing energy until a fracture was obtained.
The data was filtered and analyzed using MATLAB and the included Signal Processing Toolbox 9.2. The actual acceleration due to gravity was obtained from each test and used to calculate the actual energy induced into the system. All specimen were imaged by computed tomography (CT) and an european forearm phantom (EFP) was used during the CTs to allow for calibration and calculation of the bone mineral density (BMD). All data was then loaded into SPSS Statistics (version 29(241), IBM Armonk, NY, USA) for assessment. A significance level of $0\,05$ was set prior to testing for normality and performing a one-way analysis of variance (ANOVA) test.

III. Results

The specimens used in the main test series (8 female, 14 male, 2 unknown) had a mean BMD of $106.22\,\mathrm{mg/cm^3}\pm45.51$. 23 of 24 specimens ($95.83\,\%$) resulted in a desired fracture pattern. 19 of the 23 desired fracture patterns ($82.61\,\%$) resulted in their intended fracture patterns. The mean fracture energy was $51.25\,\mathrm{J}\pm12.08$, with a mean acceleration of $5.95\,\mathrm{m/s^2}\pm0.67$.
A lateral split fracture pattern was achieved in$12.50\,\%$ of specimens($\mathrm{n}\,=\,3$). These had a mean fracture energy of $46.38\,\mathrm{J}\pm11.48$. Bicondylar split fracture patterns were created in $45.83\,\%$ of the specimens ($\mathrm{n}\,=\,11$), with a mean fracture energy of $48.93\,\mathrm{J}\pm12.43$. Medial split fracture patterns were created in$37.50\,\%$ of specimens ($\mathrm{n}\,=\,9$). The medial split fractures had a mean fracture energy of $56.57\,\mathrm{J}\pm11.89$. A table containing the specimen list and specimen specific info can be found in Appendix 7
A one-way ANOVA test was performed to understand the relation between all variables and the resulting fracture pattern. Only the intended fracture pattern had a statistically significant ($\mathrm{p}<0.001$) correlation to the resulting fracture pattern. There was a statistically significant correlation between fracture energy and specimen trabecular BMD ($\mathrm{p}=0.025$), showing that higher BMD specimen require higher energy impacts to create a fracture.

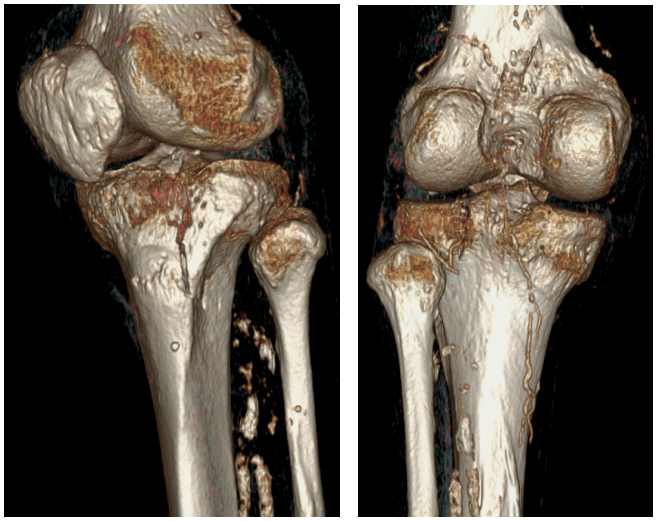

Fig. 1: Specimen AG-1085-L: Anterolateral (Left) and Posterior (Right) views of 3D rendering

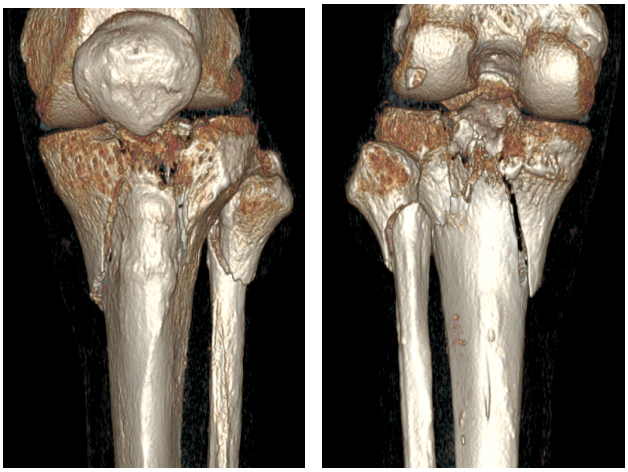

Fig. 2: Specimen AG-2131-L: Anterior (Left) and Posterior (Right) views of 3D rendering. Bicondylar split fracture.

IV. Discussion

The goal of this project is to develop a standardized fracture model for multiple tibial plateau fracture patterns. The objectives are to reliably reproduce the desired fracture patterns with minimal soft tissue damage, using cortical weakening to predetermine the breaking points and kick start fracture line propagation. In an effort to gain a deeper understanding of the custom built drop tower, an uniaxial accelerometer was affixed to the sledge and the fall acceleration recorded for calculation of the actual energy induced by the impact.
The present study shows that creation of the desired tibial plateau fracture patterns while minimally damaging the soft tissue mantel in ethanol-glycerine preserved specimens is possible through selective cortical weakening and axial compression with a sufficiently high energy impact. The resulting fractures have life-like propagation of the fracture lines and the associated concomitant injuries often seen with TPFs. The consistent and reproducible fractures are suitable

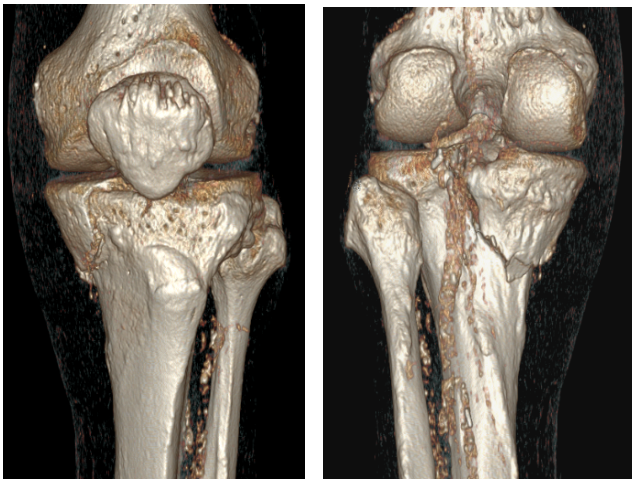

Fig. 3: Specimen AG-1074-L: Anterior (Left) and Posterior (Right) views of 3D rendering. Medial split fracture.

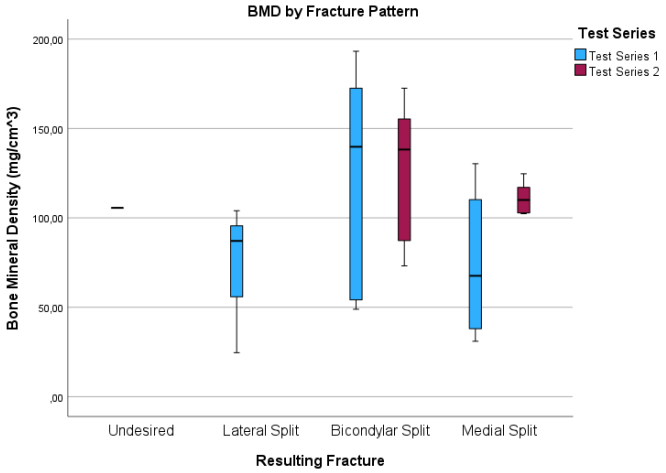

Fig. 4: Trabecular BMD by resulting fracture pattern

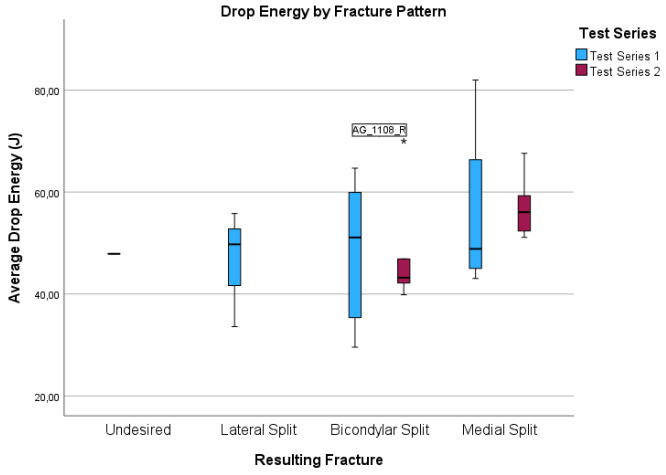

Fig. 5: Drop Energy by resulting fracture pattern

for use in surgical training courses and some biomechanical testing applications. For extensive biomechanical testing, more homogeneous fragmentation may be desired, and this is likely

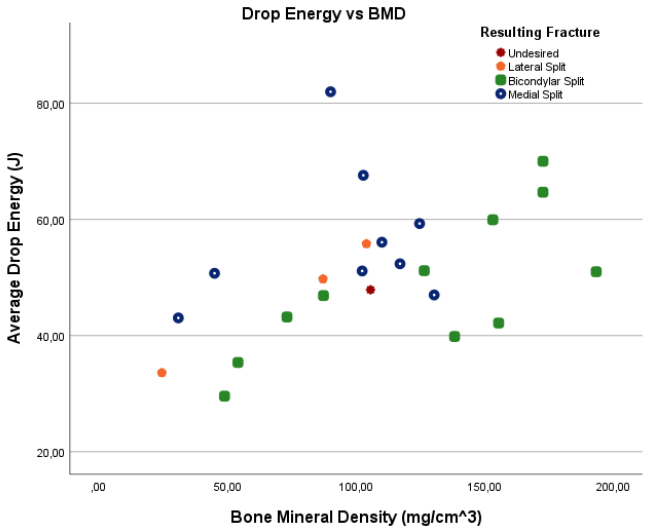

Fig. 6: Drop energy versus trabecular BMD

achievable with more extensive cortical weakening and further defining of the fragment's desired shape.

With $95.83\,\%$ of the fractures resulting in a desirable fracture pattern, and 19 of the 23 ($82.61\,\%$) desirable fractures resulting in their intended fracture pattern, the results show a reliable and reproducible method for producing fracture patterns. Three of the four unintended fracture patterns were bicondylar fracture patterns as opposed to the desired unicondylar pattern and the other resulted in a lateral fracture pattern instead of the medial that was intended.

Cortical bone after ethanol-glycerine fixation [15] absorbs less energy. In [16] distal humerus fractures are created in ethanol-glycerine preserved specimens. These specimens had a mean BMD of $118\,\mathrm{mg/cm^3}\pm48$ and a mean fracture energy of $17.8\,\mathrm{J}\pm9.1$ [16], similar to the specimen in this study, yet Schmoelz's fractures were created by material testing machine. This results in a single force being applied and increased until a fracture occurs. Wegmann created distal radius fractures [13] with the custom drop-test bench developed by Wegmann and Harbrecht [12], [13], [17], [18]. Fresh-frozen distal radius fractures were created with a mean fracture energy of $134.7\,\mathrm{J}\pm14.4$.

The specimens of this investigation have a similar BMD and fracture energy to the ethanol-glycerine preserved specimens in [16] and the reduced energy in comparison to [13] could attributed to a number of factors including the ethanol-glycerine preservation of the specimens and the predetermined breaking points chiseled into the tibial plateau that lowered the necessary energy for fracture production. The higher energy of this investigation than in [16] can be attributed to the larger surface area and weight bearing responsibilities of the tibia.

V. Conclusion

This research aimed to develop a standardized fracture model for producing a variety of tibial plateau fracture patterns. With the selective determining of fracture patterns and cortical bone weakening, three desired fracture patterns were created in $95.83\,\%$ of the ethanol-glycerine fixed specimens.

Mean fracture energy was measured to be $51.25\,\mathrm{J}\pm12.08$ and the specimens have a mean BMD of $106.22\,\mathrm{mg/cm^3}\pm45.51$. This study finds that replicating common injury mechanisms and predetermining breaking points through selective weakening of the cortical bone allow for the creation of life-like tibial plateau fracture patterns.

APPENDIX A
SPECIMEN SUMMARY

Tibial Plateau Fracture Specimens

Specimen Number	Specimen Gender	Specimen Age	BMD (mg/cm^3)	Intended Fracture	Acceleration (m/s^2)	Mass Added (kg)	Drop Height (m)	Drop Count	Fracture Energy (J)	Resulting Fracture	Test Series
AG_0028_R	Male	82	105.58	Lateral Split	5.99	15.50	0.40	8	47.88	Undesired	1
AG_0031_R	Female	98	30.97	Medial Split	5.38	15.50	0.40	1	43.04	Medial Split	1
AG_1062_L	Male	92	45.03	Medial Split	6.34	15.50	0.40	1	50.72	Medial Split	1
AG_1062_R	Male	92	54.12	Lateral Split	5.71	11.00	0.40	3	35.37	Bicondylar Split	1
AG_1083_L	Male	81	153.07	Bicondylar Split	6.66	15.50	0.45	3	59.94	Bicondylar Split	1
AG_1083_R	Male	81	172.52	Bicondylar Split	7.19	15.50	0.45	4	64.68	Bicondylar Split	1
AG_1085_L	Male	84	104.00	Lateral Split	6.20	15.50	0.45	3	55.8	Lateral Split	1
AG_2016_R	Female	84	87.13	Lateral Split	5.53	15.50	0.45	3	49.74	Lateral Split	1
AG_2021_L	Female	83	48.90	Lateral Split	4.77	11.00	0.40	1	29.57	Bicondylar Split	1
AG_2021_R	Female	83	24.57	Lateral Split	5.25	11.50	0.40	2	33.6	Lateral Split	1
AG_2044_L	Male	78	130.29	Medial Split	5.87	15.50	0.40	5	46.99	Medial Split	1
AG_2075_L	Female	86	126.43	Bicondylar Split	5.69	15.50	0.45	2	51.17	Bicondylar Split	1
AG_2075_R	Female	86	193.20	Bicondylar Split	5.67	15.50	0.45	2	50.99	Bicondylar Split	1
AG_A001_L	Unknown	Unknown	90.08	Medial Split	6.01	18.25	0.60	2	81.97	Medial Split	1
AG_1074_L	Male	73	102.79	Medial Split	6.46	18.75	0.45	2	67.59	Medial Split	2
AG_1074_R	Male	73	117.03	Medial Split	5.63	18.75	0.40	10	52.36	Medial Split	2
AG_1101_R	Male	76	124.63	Medial Split	7.41	15.50	0.40	3	59.28	Medial Split	2
AG_1108_R	Male	69	172.53	Bicondylar Split	7.00	15.50	0.50	4	70	Bicondylar Split	2
AG_1125_L	Female	62	102.34	Medial Split	6.39	15.50	0.40	2	51.12	Medial Split	2
AG_2004_R	Male	71	87.32	Bicondylar Split	5.86	15.50	0.40	2	46.88	Bicondylar Split	2
AG_2131_L	Male	83	155.32	Bicondylar Split	5.27	15.50	0.40	2	42.16	Bicondylar Split	2
AG_2131_R	Male	83	110.00	Medial Split	6.23	15.50	0.45	4	56.07	Medial Split	2
AG_8088_R	Female	85	73.15	Lateral Split	5.40	15.50	0.40	3	43.2	Bicondylar Split	2
AG_A002_L	Unknown	Unknown	138.22	Bicondylar Split	4.98	15.50	0.40	1	39.84	Bicondylar Split	2

Fig. 7: Specimen overview for tibial plateau fracture creation

ACKNOWLEDGMENT

The authors would like to thank the cadaver donors, Werner Schmoelz, Eliane Rupp, the Biomechanics laboratory at the Medical University of Innsbruck, and the Health & Medical Technologies and Mechatronics departments at the Management Center Innsbruck.

REFERENCES

[1] S. Malik, T. Herron, A. Mabrouk, and N. Rosenberg, "Tibial plateau fractures," *Tibial Plateau Fractures*, pp. 1–178, 9 2022. [Online]. Available: https://www.ncbi.nlm.nih.gov/books/NBK470593/

[2] C. M. S. II, J. P. Szatkowski, and J. T. Riehl, *Tibial Plateau Fracture. Tibia Pathology and Fractures.*, D. D. Nikolopoulous, G. K. Safos, and J. Michos, Eds., 2020. [Online]. Available: www.intechopen.com

[3] A. M. Ali, M. Saleh, S. Bolongaro, and L. Yang, "Experimental model of tibial plateau fracture for biomechanical testing," *Journal of Biomechanics*, vol. 39, pp. 1355–1360, 2006.

[4] S. A. Bini, C. C. Chung, S. A. Wu, and E. N. Hansen, "Tibial mechanical axis is nonorthogonal to the floor in varus knee alignment," *Arthroplasty Today*, vol. 8, pp. 237–242, 4 2021.

[5] J. Mthethwa and A. Chikate, "A review of the management of tibial plateau fractures," *Musculoskeletal Surgery*, vol. 102, pp. 119–127, 8 2018.

[6] T. Shimizu, T. Sawaguchi, D. Sakagoshi, K. Goshima, K. Shigemoto, and H. Yu, "Geriatric tibial plateau fractures: Clinical features and surgical outcomes."

[7] C. W. Kim, C. R. Lee, K. C. An, H. C. Gwak, J. H. Kim, L. Wang, and D. G. Yoon, "Predictors of reduction loss in tibial plateau fracture surgery: Focusing on posterior coronal fractures," *Injury*, vol. 47, pp. 1483–1487, 7 2016.

[8] M. J. Weaver, M. B. Harris, A. C. Strom, R. M. Smith, D. Lhowe, D. Zurakowski, and M. S. Vrahas, "Fracture pattern and fixation type related to loss of reduction in bicondylar tibial plateau fractures," *Injury*, vol. 43, pp. 864–869, 6 2012.

[9] A. Millán-Billi, M. Gómez-Masdeu, E. Ramírez-Bermejo, M. Ibañez, and P. E. Gelber, "What is the most reproducible classification system to assess tibial plateau fractures?" *International Orthopaedics*, vol. 41, pp. 1251–1256, 6 2017.

[10] K. Hua, X. Jiang, Y. Zha, C. Chen, B. Zhang, and Y. Mao, "Retrospective analysis of 514 cases of tibial plateau fractures based on morphology and injury mechanism," *Journal of Orthopaedic Surgery and Research*, vol. 14, 8 2019.

[11] S. N. Maripuri, P. Rao, A. Manoj-Thomas, and K. Mohanty, "The classification systems for tibial plateau fractures: How reliable are they?" *Injury*, vol. 39, pp. 1216–1221, 2008.

[12] K. Wegmann, V. Rausch, K. J. Burkhart, M. Hackl, T. Leschinger, and L. Müller, "Advanced surgical trauma care course – evaluation of a fracture simulation course concept with intact soft tissue," *Zeitschrift für Orthopädie und Unfallchirurgie*, vol. 158, pp. 291–297, 6 2020. [Online]. Available: http://www.thieme-connect.de/DOI/DOI?10.1055/a-0983-8322

[13] K. Wegmann, A. Harbrecht, M. Hackl, S. Uschok, T. Leschinger, and L. P. Müller, "Inducing life-like distal radius fractures in human cadaveric specimens: a tool for enhanced surgical training," *Archives of Orthopaedic and Trauma Surgery*, vol. 140, pp. 425–432, 2020. [Online]. Available: https://doi.org/10.1007/s00402-019-03313-5

[14] J. R. Funk, R. W. Rudd, J. R. Kerrigan, and J. R. Crandall, "The line of action in the tibia during axial compression of the leg," *Journal of Biomechanics*, vol. 40, pp. 2277–2282, 1 2007.

[15] S. Unger, B. Blauth, and W. Schmoelz, "Effects of three different preservation methods on the mechanical properties of human and bovine cortical bone," *Bone*, vol. 47, pp. 1048–1053, 12 2010.

[16] W. Schmoelz, J. P. Zierleyn, R. Hoermann, and R. Arora, "Surgery standardized fracture creation in the distal humerus and the olecranon for surgical training and biomechanical testing," *Archives of Orthopaedic and Trauma Surgery*, vol. 142, pp. 3853–3861, 2022. [Online]. Available: https://doi.org/10.1007/s00402-021-04286-0

[17] K. Wegmann, K. Engel, K. J. Burkhart, M. Ebinger, R. Holz, G.-P. Brüggemann, and L. P. Müller, "Sequence of the essex-lopresti lesion-a high-speed video documentation and kinematic analysis," *Acta Orthopaedica*, vol. 85, pp. 177–180, 2014.

[18] A. Harbrecht, J. Knifka, N. Ott, K. Wegmann, and L. P. Müller, "Inducing life-like fractures in cadaveric human specimens - the new fracture simulation machine of the department of orthopaedics and trauma surgery of the university hospital of cologne," pp. 36–38, 8 2020.

Justin Combs is a Master's Student with the Department of Medical and Health Technologies, MCI, Innsbruck, Austria. He is taking this course as part of the curriculum for the Medical Technologies Master's Program.